ACCOUNTS of chemical research

Article

pubs.acs.org/accounts

Plasmonic Vesicles of Amphiphilic Nanocrystals: Optically Active Multifunctional Platform for Cancer Diagnosis and Therapy

Jibin Song,[†,‡] Peng Huang,[†] Hongwei Duan,*[,‡] and Xiaoyuan Chen*[,†]

[†]Laboratory of Molecular Imaging and Nanomedicine (LOMIN), National Institute of Biomedical Imaging and Bioengineering (NIBIB), National Institutes of Health (NIH), Bethesda, Maryland 20892, United States

[‡]School of Chemical and Biomedical Engineering, Nanyang Technological University, 70 Nanyang Drive, 637457 Singapore

CONSPECTUS: Vesicular structures with compartmentalized, water-filled cavities, such as liposomes of natural and synthetic amphiphiles, have tremendous potential applications in nanomedicine. When block copolymers self-assemble, the result is polymersomes with tailored structural properties and built-in releasing mechanisms, controlled by stimuli-responsive polymer building blocks. More recently, chemists are becoming interested in multifunctional hybrid vesicles containing inorganic nanocrystals with unique optical, electronic, and magnetic properties. In this Account, we review our recent progress in assembling amphiphilic plasmonic nanostructures to create a new class of multifunctional hybrid vesicles and applying them towards cancer diagnosis and therapy.

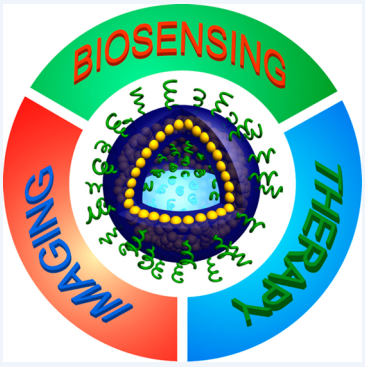

Localized surface plasmon resonance (LSPR) gives plasmonic nanomaterials a unique set of optical properties that are potentially useful for both biosensing and nanomedicine. For instance, the strong light scattering at their LSPR wavelength opens up the applications of plasmonic nanostructures in single particle plasmonic imaging. Their superior photothermal conversion properties, on the other hand, make them excellent transducers for photothermal ablation and contrast agents for photoacoustic imaging. Of particular note for ultrasensitive detection is that the confined electromagnetic field resulting from excitation of LSPR can give rise to highly efficient surface enhanced Raman scattering (SERS) for molecules in close proximity. We have explored several ways to combine well-defined plasmonic nanocrystals with amphiphilic polymer brushes of diverse chemical functionalities. In multiple systems, we have shown that the polymer grafts impart amphiphilicity-driven self-assembly to the hybrid nanoparticles. This has allowed us to synthesize well-defined vesicles in which we have embedded plasmonic nanocrystals in the shell of collapsed hydrophobic polymers. The hydrophilic brushes extend into external and interior aqueous environment to stabilize the vesicular structure. More importantly, we have demonstrated that strong interparticle coupling greatly enhances the optical properties (scattering, photothermal conversion, and SERS) in plasmonic vesicles. In combination with the loading capacity of the vesicles, this technology can provide unique opportunities for integrated diagnosis and therapy, multimodality combination therapy, and imaging-guided therapy. One key property differentiating the plasmonic vesicles from other vesicular structures containing nanocrystals is that we can tailor the interparticle coupling and disintegration of the plasmonic vesicles by altering structural parameters and conformational changes of the covalently bound polymer brushes. This gives us tremendous flexibility to engineer plasmonic vesicles for ultrasensitive detection and targeted therapy. Through bringing together advances in nanochemistry, polymer chemistry, self-assembly, and nanophotonics, we expect to further expand our capability of tailoring optical and structural characteristics of plasmonic vesicles to address challenges in medical settings.

1. INTRODUCTION

Plasmonic metal nanostructures with unique optical properties defined by localized surface plasmon resonance (LSPR) are of considerable fundamental and technological interest for bioimaging, nanomedicine, biosensing, and surface enhanced spectroscopy.[1−5] LSPR of plasmonic nanostructures is strongly dependent on intrinsic structural parameters (size, shape, and chemical composition) and dielectric properties of their immediate environment (refractive index and interparticle spacing of neighboring nanoparticles).[2,6,7] The dependence on intrinsic properties has stimulated the rapid development of customized wet-chemical synthesis of plasmonic nanostructures.[8,9] The dependence on immediate external environment, on the other hand, forms the fundamental basis of plasmonic nanosensors, in which biological stimuli of interest induce changes in refractive index or interparticle spacing of nanoparticle ensembles to produce colorimetric or spectroscopic changes.[10,11]

Excited LSPR arising from collective oscillation of free conduction electrons dissipates energy through Mie scattering and absorption-associated heat conversion processes.[12] The photobleaching-free light scattering offers the possibility of miniaturizing plasmonic sensors down to single particle level. The efficient photothermal conversion property holds great promise in photothermal therapy (PTT) and photoacoustic imaging (PAI), in which the ultrasound wave resulting from thermal expansion is used to produce 3D images.[13−16] The

Received: February 2, 2015
Published: July 2, 2015

DOI: 10.1021/acs.accounts.5b00059
Acc. Chem. Res. 2015, 48, 2506−2515

broadly tailorable LSPR of plasmonic nanostructures or their ensembles makes it possible to match LSPR with laser wavelengths for maximal therapeutic outcome and imaging sensitivity.[6,17,18] A particular spectral window of interest for *in vivo* applications is in the near-infrared (NIR) range (650−900 nm), in which water and soft tissue cause minimal light absorption, leading to better light penetration.[19,20] Furthermore, LSPR gives rise to a confined electromagnetic field surrounding plasmonic nanostructures, which greatly amplifies surface enhanced Raman scattering (SERS) signals of molecules directly attached on their surfaces.[21−24] The degree of enhancement is closely related to the LSPR and geometry of plasmonic nanostructures, the spectral profile and adsorption sites of Raman molecules, and the excitation wavelength of the laser light source.[25,26] Also interesting is that strongly coupled nanoparticles exhibit a locally enhanced field at the nanogap junctions and interstitial spaces, leading to more efficient signal amplification than individual nanoparticles.[24,27]

In light of the distinctively different optical and spectroscopic properties of individual and coupled plasmonic nanostructures, major research efforts have been made to develop well-defined ensembles of plasmonic nanostructures theoretically and experimentally to achieve improved understanding and better uses of plasmonic coupling.[2,28] A wide spectrum of small molecular, biomolecular, and polymeric coatings have been employed to direct self-assembly of plasmonic nanostructures.[29−33] While biomolecules such as DNA and antibody/antigen offer high specificity based on their natural recognition ability, polymeric coatings feature diverse chemical functionality and well-established self-assembly systems, fueled by recent advances in polymer chemistry and long-standing research interest in self-assembly of block copolymers in bulk phases and selective solvents.

Our recent research has led to the development of a new class of plasmonic ensembles, that is, plasmonic vesicles, assembled from amphiphilic polymer brush coated nanoparticles.[34−41] The plasmonic vesicles are characteristic of the collective optical and spectroscopic properties of nanoparticle ensembles and the enclosed cavity structure similar to that of liposomes and polymersomes. In this Account, we will summarize the development in synthesis of amphiphilic polymer brush-grafted nanocrystals, key findings in controlling the properties of plasmonic vesicles, and the applications of plasmonic vesicles as optically active multifunctional platforms for highly desirable cancer applications such as integrated diagnosis and therapy, multimodality combination therapy, and imaging-guided therapy.

2. TAILORED SYNTHESIS OF AMPHIPHILIC PLASMONIC NANOCRYSTALS

Amphiphilic plasmonic nanocrystals have a "soft" shell of amphiphilic polymers grafted on a "hard" core of metallic nanocrystals.[35,42,43] Previous research has demonstrated that self-assembly of amphiphilic block copolymer is strongly affected by both thermodynamic and kinetic factors, with the former closely related to polymer structures such as molecular weight and relative ratios of hydrophilic and hydrophobic blocks and the latter largely dependent on assembly conditions. Similarly, in order to simultaneously control the structural and optical properties of plasmonic vesicles, it is necessary to obtain well-defined building blocks with precisely controlled amphiphilic polymer brushes grafted on high-quality nanocrystals. There are well-established wet-chemical methods to synthesize monodispersed plasmonic nanocrystals, primarily Au and Ag nanostructures, with tailored sizes and shapes and thus optical properties.[9] Polymer brushes are typically grafted on nanoparticle cores via two approaches: "grafting to" by attaching end-functionalized polymers on nanoparticle surfaces and "grafting from" by growing polymer chains from surface-anchored initiators.[35,43] Amphiphilic polymer brushes on the nanocrystals can be either mixed brushes of hydrophilic and hydrophobic homopolymers (Figure 1a,b) or homobrushes of

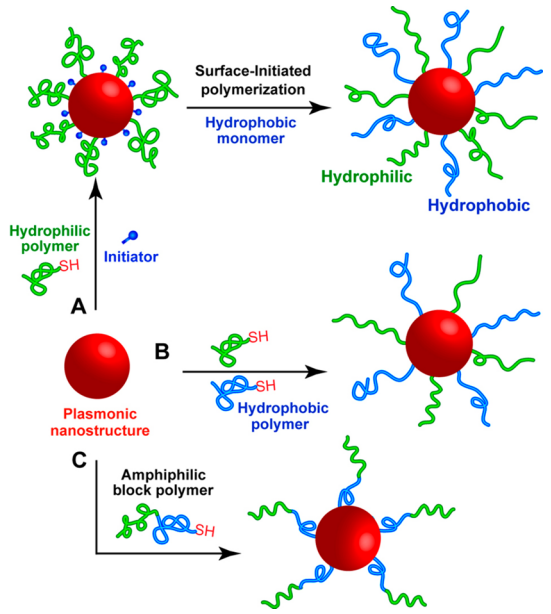

Figure 1. Schematic illustration of the synthesis of amphiphilic plasmonic nanocrystals grafted with polymer brushes: (a) tandem "grafting to" (coadsorption of hydrophilic homopolymers and initiators) and "grafting from" (surface-initiated polymerization) methods; (b) coadsorption of hydrophilic and hydrophobic polymer ending with a thiol end group; (c) "grafting to" of amphiphilic diblock copolymer ending with a thiol end group.

amphiphilic block copolymers with hydrophilic and hydrophobic blocks covalently jointed together (Figure 1c). Zubarev et al. pioneered the synthesis of amphiphilic plasmonic nanocrystals by chemically linking V-shaped polybutadiene-*b*-poly(ethylene oxide) (PEO) and polystyrene (PS)-*b*-PEO on 2 nm Au nanoparticles (AuNPs).[44]

We recently developed a new strategy based on tandem "grafting to" and "grafting from" reactions to synthesize plasmonic nanocrystals coated with mixed homopolymer brushes of diverse chemical functionalities.[35−37,43] In our strategy (Figure 1a), one homopolymer (i.e., the hydrophilic one) and polymerization initiator are first attached together on plasmonic nanocrystals through metal−sulfur bond, and the coated nanocrystals are further used as macroinitiators for the surface-initiated polymerization to grow the second polymer (i.e., the hydrophobic one) on the nanocrystals. Poly(ethylene glycol) (PEG) is widely used in biotechnology and nanomedicine to create nonfouling surfaces and serve as flexible spacers for targeting ligands and becomes the primary hydrophilic homopolymer of choice in our design. Recent advances in living polymerization methods such as atom transfer radical polymerization (ATRP) and organocatalytic ring-opening polymerization (ROP) have made it possible for the controlled polymerization of a wide spectrum of vinyl-based

DOI: 10.1021/acs.accounts.5b00059
Acc. Chem. Res. 2015, 48, 2506−2515

and cyclic monomers.[34,35,45,46] We have demonstrated that the tandem "grafting to" and "grafting from" strategy is compatible with plasmonic nanocrystals of different sizes, shapes, and surface chemistry, leading to the growth of hydrophobic polymers with desired stimuli-responsiveness and biodegradability on the nanocrystals.[23,34−37,43] It should be mentioned that since polymers are attached on the nanocrystals via a metal−sulfur bond, which becomes labile at high temperature (>60 °C), surface-initiated polymerization needs to be done under relatively mild conditions.[34] This is also why we developed surface-initiated organocatalytic ROP for the growth of biodegradable polyester and polycarbonate brushes, which traditionally are polymerized by metal-catalyzed ROP at high temperature (>100 °C).[34] Importantly, our strategy allows for controlling the MW and relative ratio of the mixed brush at a high graft density (0.4−0.5 chain/nm^2), as shown for the combinations of PEG/poly(methyl methacrylate) (PMMA)[35] and PEG/polylactide (PLA)[34] among others.[23,36,37,43] Mixed brushes of homopolymers also can be formed by grafting end-functionalized hydrophobic and hydrophilic polymer simultaneously, as shown in Figure 1b. This approach based on "grafting to" reactions, however, typically leads to low graft density (<0.2 chain/nm^2) because of the competitive binding and steric hindrance effect between the polymer chains.[34] Nie and co-workers took a different approach and prepared amphiphilic plasmonic nanocrystals by grafting amphiphilic block copolymers with an anchoring thiol group at the end of their hydrophobic blocks on nanocrystals (Figure 1c).[38,40,41,47] Essential structural parameters of the homobrush such as relative ratios of hydrophilic and hydrophobic components and MW can be simply tuned by tailoring the block copolymer structure. Also interesting is that this approach leads to amphiphilic nanocrystals with hydrophilic and hydrophobic blocks locally phase separated, unlike the mixed homopolymer brushes, although low graft density (~0.1 chain/nm^2) is obtained.[41]

3. SELF-ASSEMBLY AND OPTICAL ENGINEERING OF PLASMONIC VESICLES

Self-assembly of amphiphilic block copolymers is driven by self-aggregation of hydrophobic blocks in aqueous environments, and the hydrophilic blocks serve to limit the aggregation at certain stages and stabilize the resulting structures. It turns out that the methods used for self-assembly of block copolymers are also applicable to amphiphilic nanocrystals. We started with the film rehydration method,[34−37] which is commonly used to produce liposomes and polymersomes. We reason that forming a thin film of closely packed nanocrystals by slow evaporation of the common solvent for the hydrophilic and hydrophobic homopolymers provides an energetically favorable state to form vesicles by rolling over of the detached thin film upon rehydration.[35,36] Nie et al. later demonstrated that gradual change of the solvent quality from common solvents to selective solvents (i.e., water) for hydrophilic polymers also led to integral plasmonic vesicles.[39] Notably, no matter which method was used, the shell of the resulting vesicles always appeared as a monolayer array of closely attached nanocrystals (Figure 2a,b), unlike the bilayer structure found in liposomes and polymers.[48,49] As illustrated in Figure 2c, it is assumed that hydrophobic brushes collapse to form the shell of the vesicle and hydrophilic brushes undergo conformational rearrangement to face aqueous environments on either side of the shell, with the plasmonic nanocrystals embedded in the shell. Since

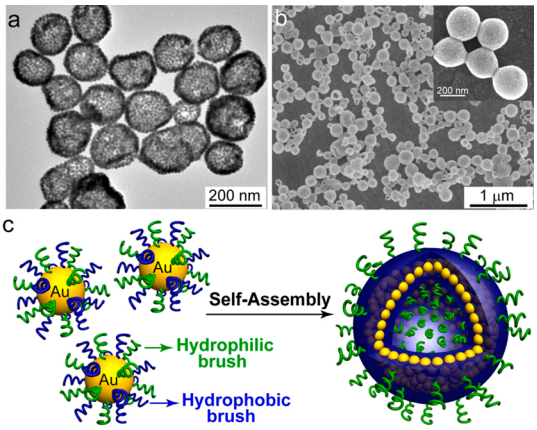

Figure 2. Transmission electron microscopy (TEM, a) and scanning electron microscopy (SEM, b) images of the vesicles formed by 14 nm AuNPs coated with PEG and a copolymer of methyl methacrylate (MMA) and 4-vinylpyridine (VP). (c) Schematic illustration of self-assembly of amphiphilic Au nanoparticles coated with mixed brushes of hydrophilic and hydrophobic homopolymers into a vesicle. Reprinted with permission from refs 35 and 36. Copyright 2012 and 2011 American Chemical Society.

the sizes of the nanocrystals used in these studies are all comparable to or larger than the dimension of the polymers, we reason that forming a shell of bilayer structure would have trapped a large fraction of the hydrophilic brushes in the shell, which is thermodynamically unfavorable, thus making the nanoparticle adopt the monolayer arrangement.

The promise of plasmonic vesicles for biomedical applications lies in the ability to tailor their optical and spectroscopic properties. We have found that close packing of plasmonic nanocrystals in the vesicle shell led to strong interparticle plasmonic coupling. As shown in Figure 3a, LSPR of plasmonic vesicles, assembled from 14 nm AuNPs grafted with PEG and a copolymer (PMMAVP) of methyl methacrylate (MMA) and 4-vinylpyridine (VP), exhibits a clear red-shift relative to that of individual nanoparticles (AuNP@PEG/PMMAVP). Single particle imaging (Figure 3b) by dark field microscopy reveals strong red light scattering from the vesicles, which further supports the strong coupling of nanoparticles because 14 nm nanoparticles have negligible light scatting. The covalently bound polymer brushes enables tailoring interparticle spacing by their conformational changes.[36] For example, when pH was changed from 7.4 to 5.0, the hydrophobic PMMAVP copolymer became hydrophilic because of protonation of the pH-sensitive pyridine group (pK_a = 5.4), leading to dissociation of the vesicles into individual nanoparticles or small clusters.[36] This process can be continuously monitored by plasmonic imaging, which showed gradual blue shifts of the scattering spectra (inset of Figure 3b). In the vesicles of Raman-encoded Au nanorods (AuNRs) with PEG and PLA brushes (AuNR@PEG/PLA), the interparticle coupling not only caused significant red-shifts of both transverse and longitudinal LSPR of AuNRs (Figure 3c) but also afforded a considerable enhancement of SERS signal by a factor of 24, with an ensemble-averaged enhancement factor of 5.7 × 10^6.[34] The other key structural factor that we investigated is the relative ratio of hydrophobic and hydrophilic brushes. The results showed that increase of the ratio, while maintaining the graft density, led to stronger interparticle coupling, evidenced by a further red shift of the LSPR peak.[34,37] It is believed that

DOI: 10.1021/acs.accounts.5b00059
Acc. Chem. Res. 2015, 48, 2506−2515

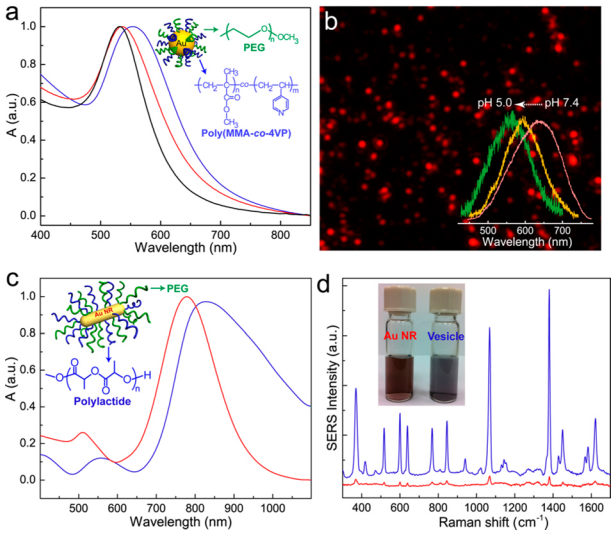

Figure 3. (a) UV−vis spectra of 14 nm Au@PEG/PMMAVP in chloroform (black line) and Au@PEG/PMMAVP vesicle in pH = 5.0 (red line) and 7.0 (blue line) aqueous solutions. (b) Dark-field image of Au@PEG/PMMAVP vesicles in pH = 7.0 aqueous dispersion (inset shows scattering spectra of the vesicle at different pH). (c) UV−vis spectra of AuNR@PEG/PLA in chloroform (red line) and AuNR@PEG/PLA vesicles in aqueous medium (blue line). (d) SERS spectra of the AuNR@PEG/PLA vesicles and AuNRs (red line) tagged with Raman reporter 2-naphthalenethiol (blue line). Inset shows photographs of AuNR (left) and vesicle (right) dispersion. Reprinted with permission from ref 34 and 36. Copyright 2013 and 2012 American Chemical Society.

reducing the number of hydrophilic grafts reduces the steric hindrance for the association of nanoparticles and gives rise to more efficient packing of the nanoparticle cores and hence stronger coupling.

Plasmonic properties of the vesicles coated with amphiphilic block copolymers can also be systematically tuned by controlling the interparticle spacing. Nie and co-workers made systematic studies on the self-assembly of AuNPs coated with PEG-*b*-polystyrene (Au@PEG-*b*-PS) and found that vesicles were preferably formed when the ratio of the average root-mean-square end-to-end distance (R_0) of the PS block and the size of the AuNPs (d_{Au}) is smaller than 0.5. Meanwhile, the average interparticle spacing (D_{Au}) (Figure 4) was approximately linearly dependent on the MW of the PS block, increasing from 5.7 ± 0.9 to 10.9 ± 2.9 nm with gradual increase of the PS MW from 11900 to 47300 g/mol.[41] Increases of interparticle distance reduced the degree of plasmonic coupling, as reflected by LSPR of 25 nm AuNPs blue-shifted from 568 to 549 nm.[41]

Chen, Nie, and co-workers reported biodegradable plasmonic vesicles formed by 26 nm AuNPs coated with PEG-*b*-poly(ε-caprolactone) (PCL) and discovered that dialyzing a tetrahydrofuran dispersion of the amphiphilic Au@PEG-*b*-PCL nanoparticles against water gave rise to vesicles with narrow size distributions of 192.6 ± 11.8 nm and 207.3 ± 15.7 nm at nanoparticle concentrations of 100 and 150 μg/mL, respectively.[39] Small clusters or submicrometer-sized vesicles were formed when the concentration was lower than 50 μg/mL or higher than 250 μg/mL. Thanks to the more flexible PCL chains compared with PS, the Au@PEG-*b*-PCL vesicles exhibit smaller interparticle distances and stronger coupling, as suggested by the more significant red shifts of LSPR peaks

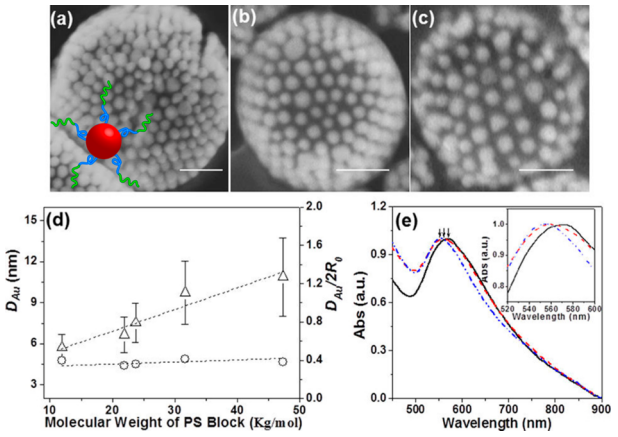

Figure 4. SEM images of plasmonic vesicles assembled from 25 nm AuNPs coated with PEG_{45}-*b*-PS_{114} (a), PEG_{45}-*b*-PS_{245} (b), and PEG_{45}-*b*-PS_{455} (c). Scale bars 100 nm. (d) The variation of interparticle spacing D_{Au} (triangle) and $D_{Au}/(2R_0)$ (circle) versus the MW of the PS block. (e) UV−vis spectra of vesicles of PEG_{45}-*b*-PS_{114} (black line), PEG_{45}-*b*-PS_{245} (red line), and PEG_{45}-*b*-PS_{455} (blue line). Reprinted with permission from ref 41. Copyright 2012 American Chemical Society.

(Figure 5a). Of particular interest for therapeutic and imaging applications is that the stronger interparticle coupling also led

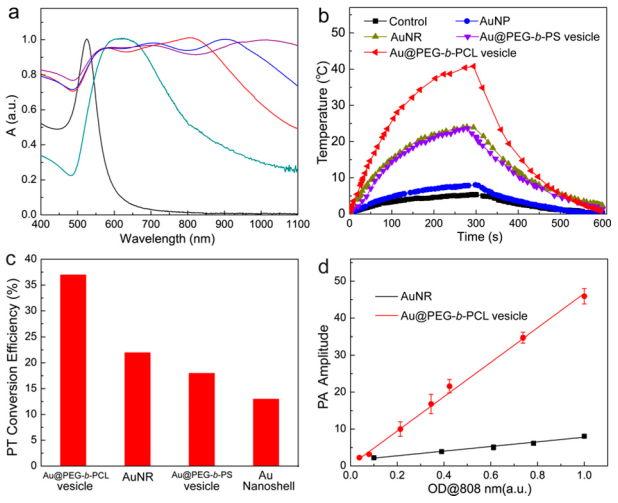

Figure 5. (a) UV−vis spectra of 26 nm AuNPs (black line), Au@PEG-*b*-PS vesicles (green line), and Au@PEG-*b*-PCL vesicles formed at nanoparticle concentrations of 100 (red line), 150 (blue line), and 250 μg/mL (purple line). (b) Temperature variation of AuNPs (at the same Au concentration as that of the Au@PEG-*b*-PCL vesicles, λ_{ex} = 808 nm), AuNRs (OD@808 nm = 1, λ_{ex} = 808 nm), Au@PEG-*b*-PS vesicles (OD@671 nm = 1, λ_{ex} = 671 nm), and Au@PEG-*b*-PCL vesicles (OD@808 nm = 1, λ_{ex} = 808 nm) as a function of irradiation time at 1 W/cm^2. (c) Photothermal conversion efficiency of different Au nanostructures. (d) Average PA intensity of AuNRs and Au@PEG-*b*-PCL at different optical density. Reprinted with permission from ref 39. Copyright 2013 Wiley-VCH.

to better photothermal conversion efficiency (η) and photoacoustic signal. At the same concentration of Au atoms (AuNPs) or optical density (other samples), the Au@PEG-*b*-PCL vesicle led to the most rapid temperature increase among AuNPs, AuNRs, and Au@PEG-*b*-PS vesicle, irradiated at the optimal excitation laser wavelength (λ_{ex}) for each sample (671 nm for Au@PEG-*b*-PS vesicles and 808 nm for others) at 1 W/

DOI: 10.1021/acs.accounts.5b00059
Acc. Chem. Res. 2015, 48, 2506−2515

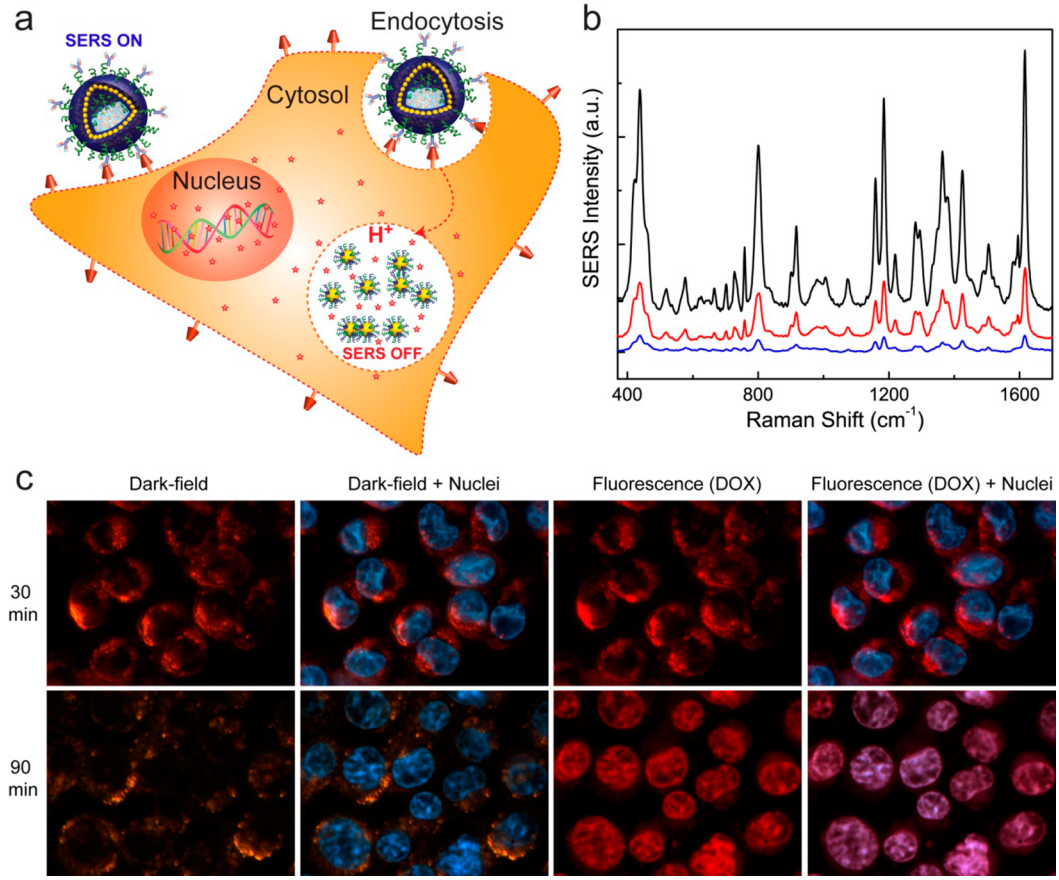

Figure 6. (a) Schematic illustration of the cellular binding and pH-regulated intracellular drug release of the SERS-encoded pH-sensitive Au@PEG/PMMAVP vesicles. (b) SERS spectra of SKBR-3 cells treated with targeted Au@PEG/PMMAVP vesicles after 30 min incubation (black line) and the postincubation spectra of the cells at 60 min (red line) and 90 min (blue line). (c) Dual dark-field and fluorescence imaging of SKBR-3 cells labeled with doxorubicin (DOX) loaded pH-responsive vesicles after 30 and 90 min incubation. Reprinted with permission from ref 36. Copyright 2012 American Chemical Society.

cm^2 for 5 min. The same trends were also found in the η values calculated for AuNRs (22%), Au nanoshells (13%), Au@PEG-*b*-PS vesicles (18%), and Au@PEG-*b*-PCL vesicles (37%). PAI records broadband acoustic waves from thermal expansion caused by pulsed laser irradiation and offers the possibility for offsetting the limitations of optical imaging caused by limited tissue penetration. Au nanostructures are under intense research as PA contrast agents because of their high optical absorption coefficient and electromagnetic field upon laser irradiation. The red shifts and broadening of LSPR induced by interparticle coupling provides the possibility to use a NIR laser for PAI, leading to increased penetration depth. The strong electromagnetic field in the conjunction areas also increases the PA signal. In this context, the Au@PEG-*b*-PCL vesicles with ultrastrong plasmonic coupling and NIR absorption led to greater PAI signal than AuNRs (Figure 5d).

An alternative strategy to prepare vesicular structures containing plasmonic nanoparticles is to load nanoparticles into the shell of vesicles (liposomes and polymersomes) or on the surface of spherical templates via noncovalent interactions.[30−33] However, the structures obtained are fundamentally different from the plasmonic vesicles in both structures and properties. In plasmonic vesicles, the covalently anchored polymer brushes on the nanoparticles offer great flexibility in tuning interparticle distance and impart stimuli-responsiveness to the vesicle by the conformational changes inherent to the brushes. This in turn allows for systematically tailoring of the plasmonic properties of the vesicles across a broad spectral range, which is essential for engineering plasmonic vesicles for ultrasensitive detection and targeted therapy.

4. MULTIFUNCTIONAL PLASMONIC VESICLES FOR CANCER DIAGNOSIS AND THERAPY

The plasmonic vesicles represent a new type of multifunctional nanoscale platform with a unique combination of structural, optical, and spectroscopic properties, which create a myriad of opportunities for biomedical applications, in particular for cancer theranostic applications that require integrated diagnostic and therapeutic functions. More specifically, the excellent SERS and PAI activity allow for sensitive detection of cancer cells if the vesicles are able to specifically recognize cancer cells; the hydrophobic shell and aqueous cavity of the vesicles provide environments for loading of therapeutic agents with different physiochemical properties (i.e., anticancer drugs and photosensitizers), which, in synergy with the photothermal therapy of the vesicles, open applications in combination cancer therapy. Also interesting is that a designed drug releasing mechanism related to disease-specific physiological conditions can be built in the vesicles by chemically tailoring the hydrophobic polymers for stimuli-triggered hydrophobic-to-hydrophilic transition or degradation. And the payload release induced by vesicle destruction can be followed up in real time

DOI: 10.1021/acs.accounts.5b00059
Acc. Chem. Res. 2015, 48, 2506−2515

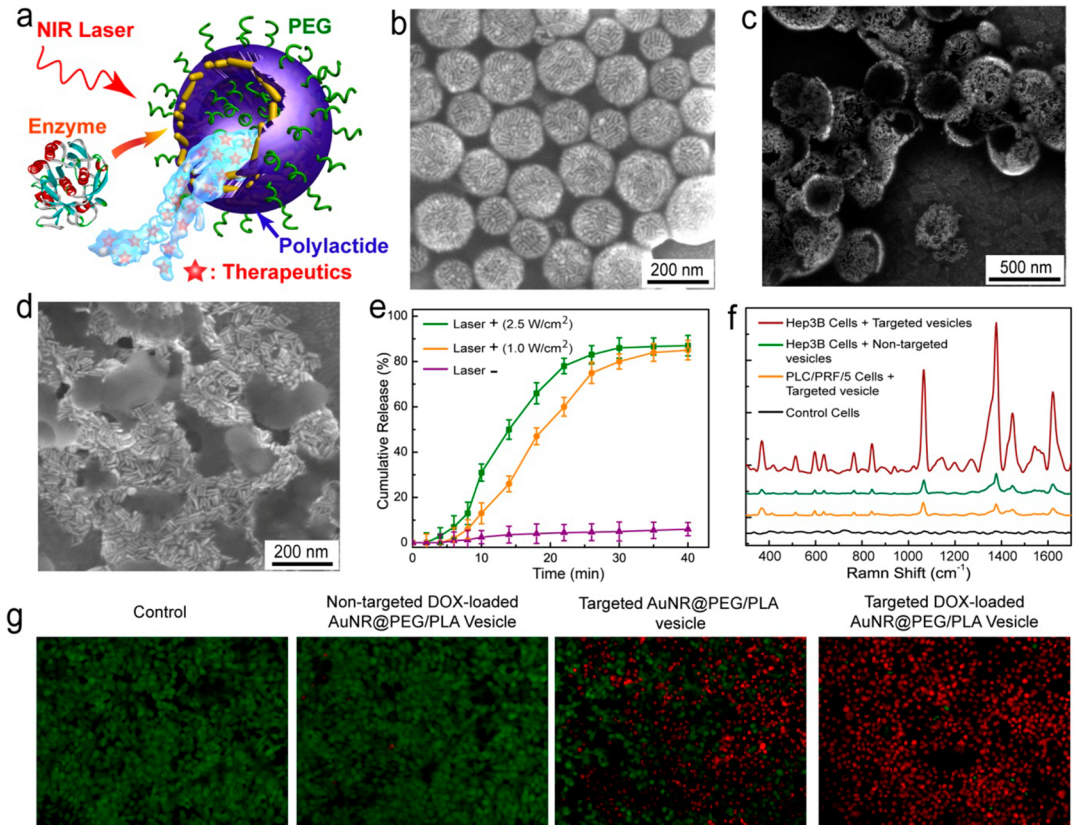

Figure 7. (a) Schematic illustration of the doxorubicin (DOX) loaded AuNR@PEG/PLA vesicles responsive to both NIR laser and enzyme. SEM (b) and TEM (c) images of AuNR@PEG/PLA vesicle. (d) SEM image of the AuNR@PEG/PLA vesicles after NIR laser irradiation at a power density of 2.5 W/cm^2 for 6 min. (e) DOX release profile of DOX-loaded AuNR@PEG/PLA vesicles treated with or without NIR laser irradiation. (f) SERS spectra of Hep3B cells labeled with targeted SERS-encoded AuNR@PEG/PLA vesicles at different concentration (number of cells/mL). (g) Fluorescence images of calcein AM/propidium iodide stained Hep3B cancer cells incubated with nontargeted doxorubicin (DOX)-loaded vesicle, targeted vesicle, and targeted DOX-loaded vesicles after 808 nm laser irradiation (1.0 W/cm^2 for 8 min). Control: laser only. Reprinted with permission from ref 34. Copyright 2013 American Chemical Society.

by taking advantage of the distinctively different scattering and SERS properties of vesicles and individual building blocks.

Our first report of using plasmonic vesicles in a biological environment is on the pH-sensitive vesicles formed by AuNP@PEG/PMMAVP.[36] There is growing interest in developing targeted drug delivery systems in response to the acidic extracellular environment of solid tumors and acidic intracellular endocytic compartments. We showed that attaching a HER2 antibody at the end of the PEG grafts enabled specific recognition of the vesicles to SKBR-3 breast cancer cells with overexpressed HER protein. As illustrated in Figure 6a, once the vesicles were taken up by the cell through endocytosis, the acidic environment in the endocytic pathway (pH 5.9−6.2 in early endosomes and pH 4.7−5.5 in late endosomes/lysosomes) caused the protonation of the pyridine groups making the hydrophobic PMMAVP (25% of vinylpyridine) hydrophilic, which was accompanied by vesicle disruption. Hence, we were able to employ the associated changes in optical signals such as blue shifts of scattering light and decrease of SERS intensity as a general independent mechanism to trace the intracellular release of payload (Figure 6b,c). This was validated by using doxorubicin (DOX) as a model drug, and the results showed the release and intracellular redistribution of DOX were correlated with the feedback of scattering light and SERS signals. The traceable drug delivery by plasmonic vesicles was further verified by light-sensitive vesicles of AuNPs coated with PEG and poly(2-nitrobenzyl acrylate).[37]

The structure of plasmonic vesicles makes it practical to couple diagnostic techniques such as SERS and PAI with therapeutic modality such as photothermal therapy, chemotherapy, and photodynamic therapy to have a localized synergistic effect, which is essential for cancer applications.[38,39] We have shown that intratumoral injection of Au@PEG-*b*-PCL vesicles in the MDA-MB-435 mice tumor model gave rise to 10-fold increase in photoacoustic intensity over that before injection, and the resulting signal was twice that observed upon the injection of Au@PEG-*b*-PS vesicles. More importantly, the Au@PEG-*b*-PCL vesicles result in much better therapeutic outcome, indicated by the rapid tumor regression after a single dose (400 μg/mL, 50 μL) and 100% survival rate of the treated mice. The Au@PEG-*b*-PCL vesicles were found accumulated prominently in the reticuloendothelial system (RES)-rich organs such as liver and spleen. After laser irradiation, the vesicles were removed from the RES on day 8. We reason that vesicle destruction after laser irradiation and degradation under physiological conditions breaks the vesicles into smaller structures facilitating their clearance. We also found no obvious inflammation or damage of major organs of treated mice, including heart, liver, spleen, lung, and kidneys, suggesting the low cytotoxicity and biocompatibility of the vesicles.[39]

SERS detects vibrational fingerprints of Raman-active molecules and holds great promise in multiplexed detection.[22,26,50,51] We explored the use of this new type of SERS-active biodegradable AuNR@PEG/PLA vesicles for targeted

DOI: 10.1021/acs.accounts.5b00059
Acc. Chem. Res. 2015, 48, 2506−2515

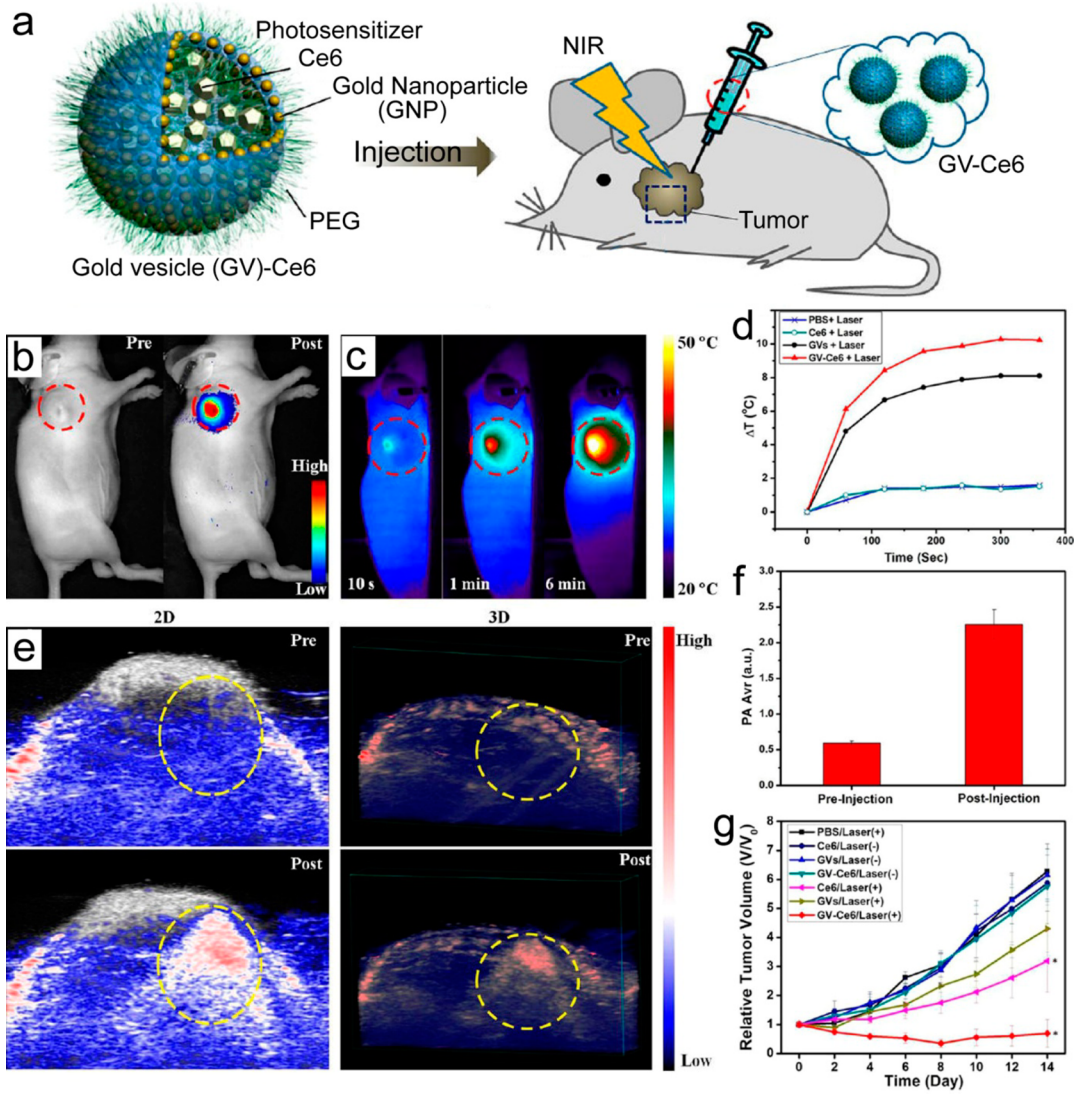

Figure 8. (a) Schematic illustration of the Ce6 loaded Au@PEG-*b*-PS vesicle for integrated photodynamic/photothermal cancer therapy. (b) Near-infrared (NIR) fluorescence image of the tumor bearing mice. (c) Infrared thermographic images of tumor-bearing mice after injection of Ce6 loaded vesicle irradiated with laser. (d) Temperature increasing profiles of the tumor at different irradiation time. Two- and three-dimensional photoacoustic (PA) image (e) and PA intensity (f) of the tumor region pre- and postinjection of vesicle. (g) Tumor growth curves of MDA-MB-435 tumor-bearing mice with different treatments. Reprinted with permission from ref 38. Copyright 2013 American Chemical Society.

cancer cell detection and combined photothermal and chemotherapy (Figure 7a).[34] It was found that the destruction of the vesicles can be initiated by both enzyme (e.g., proteinase K) that degrades PLA and laser irradiation, which "melts" the polymer shell by photothermal heating. In contrast to the slow digestion of PLA by the enzyme over more than 24 h (Figure 7b,c), laser heating led to much faster destruction, which further gave rise to rapid release (80%) of cargo molecules in 30 min (Figure 7d,e). Coupling EpCAM antibody on the vesicles enabled the targeted labeling of EpCAM-positive liver cancer cells (i.e., Hep3B cells), but not the PLC/PRF/5 cells without overexpresssion of EpCAM. The strong Raman signal of the vesicle led to ultrasensitive detection of the labeled Hep3B cells with a detection limit down to 40 cells/mL (Figure 7f). The label-free Raman spectroscopy was used to characterize cancer tissue and distinguish between normal (noncancerous) and cancerous tissues.[52,53] For example, previous results demonstrated that carotenoid and lipid composition of cancerous breast tissues exhibit significantly different Raman signal compared with the surrounding noncancerous breast tissue. Raman signal of the encoded plasmonic vesicle originates from the Raman molecules anchored on the nanocrystal surface. Thus, the Raman signal and intensity of the labeled cells is only related to the number of the endocytosed vesicles, which is not sensitive to the tissue part (cancer or noncancerous). Furthermore, there is no difference in Raman signal between the cancer and normal cells labeled with the same amount of vesicles. Moreover, a live/dead cell staining assay by green fluorescent calcein AM (live) and red fluorescent propidium iodide (dead) clearly demonstrated a synergistic effect for more efficient cell killing (100%) by the combination of a mild laser irradiation (1.0 W/cm^2) and a low dosage of DOX (0.5 μg/mL) for Hep3B cells labeled with the EpCAM-targeted vesicles.

When photosensitizer molecules (e.g., Ce6) were loaded into the Au@PEG-*b*-PS vesicles, we were able to perform combined photothermal and photodynamic therapy (Figure 8a), in which cytotoxic reactive oxygen species (ROS) generated by laser

DOI: 10.1021/acs.accounts.5b00059
Acc. Chem. Res. 2015, 48, 2506−2515

irradiation in the presence of photosensitizer and oxygen was employed for treatment.[38] In addition, trimodality imaging including NIR optical imaging that captured the Ce6 fluorescence, photothemal imaging that measured the temperature distribution, and PAI were realized by the intratumorally delivered Ce6-loaded vesicles (Figure 8b−e). Tumor temperature rapidly rose above 42 °C upon localized laser irradiation for 5 min, while negligible effect was caused to the other parts of the body (temperature increase only 1−2 °C). PAI signal in the tumor region increased to 3.8-fold of the original background signal before injection (Figure 8f), leading to clear PAI imaging of the solid tumor. Furthermore, the Ce6-loaded vesicles obviously resulted in better therapeutic outcome in comparison with the empty vesicles and free Ce6, demonstrating the advantage of combined PTT and PDT in cancer therapy.[38]

5. CONCLUSIONS AND PERSPECTIVE

In this Account, we have summarized our research progress in the past 5 years in developing well-defined amphiphilic plasmonic nanocrystals with tailored structures and their self-assembled plasmonic vesicles and exploring the preclinical tests of plasmonic vesicles for cancer diagnosis and therapy. Systematic work has been done to investigate the dependence of the structural, optical, and spectroscopic properties of plasmonic vesicles on the structural details of nanoparticle building blocks and assembly conditions. In multiple systems, we have demonstrated that plasmonic vesicles with rationally tailored structures and functions are of considerable potential for cancer applications such as imaging-guided therapy, intraoperative detection and ablation of positive tumor margins, and real-time monitoring of therapeutic outcome.

The biodegradable plasmonic vesicles that we developed provide a good starting point for clinical translation. However, practical clinical applications of the vesicles currently available are limited by their large sizes and poor understanding in pharmacokinetics (PK), pharmacodynamics (PD), and the toxicity profile. Future development should be directed toward structural optimization and more systematic preclinical examinations to address these challenges. First, the size of the plasmonic vesicles should be reduced to 50−100 nm, which will make systematic delivery possible. The current plasmonic nanostructures such as spherical nanoparticles and nanorods cannot meet this need. The use of smaller anisotropic nanostructures can possibly lead to compact vesicles with necessary optical properties. A new generation of nonmetallic plasmonic nanomaterials should also be considered since their LSPR peaks are primarily in the NIR spectral region. Second, in addition to small molecular drugs, biomacromolecular drugs such as monoclonal antibodies and therapeutic nucleic acids should be encapsulated in the aqueous cavity, which would open new possibilities for combination therapy. Recent developments in molecular biology and drug discovery have provided a library of candidates for this purpose. Third, labeling techniques that allow for noninvasive quantification of PD, PK, and biodistribution should be investigated in animal models. Fourth, amphiphilicity-driven self-assembly of nanoparticles is generally applicable for nanocrystals of diverse chemical nature and properties. Self-assembled vesicles of other functional nanocrystals such as semiconductor quantum dots and magnetic nanostructures would create new opportunities for clinical applications.

AUTHOR INFORMATION

Corresponding Authors

*H. Duan. E-mail: hduan@ntu.edu.sg.
*X. Chen E-mail: shawn.chen@nih.gov.

Author Contributions

The manuscript was written through contributions of all authors. All authors have given approval to the final version of the manuscript.

Funding

We thank the intramural research program of the National Institute of Biomedical Imaging and Bioengineering (NIBIB) for support of this work. H.D. is grateful to Singapore Ministry of Education for financial support (Tier 1 project RG47/13 and Tier3 project MOE2013-T3-1-002).

Notes

The authors declare no competing financial interest.

Biographies

Jibin Song obtained his Ph.D. degree in Chemical and Biomedical Engineering at Nanyang Technological University, Singapore, in 2014. Since 2014, he has worked with Prof. Xiaoyuan (Shawn) Chen as a postdoctoral fellow at National Institutes of Health (NIH). His research was focused on creating novel nanomaterials for drug delivery, bioimaging, and cancer therapy, including polymeric and plasmonic assemblies, quantum dots, and nano- and microparticles.

Peng Huang received his Ph.D. degree in Biomedical Engineering from the Shanghai Jiao Tong University, China, in 2012. Then he joined the Laboratory of Molecular Imaging and Nanomedicine (LOMIN) at the National Institutes of Health (NIH) as a postdoctoral fellow under the supervision of Prof. Xiaoyuan (Shawn) Chen. He has focused on the design, synthesis, and biomedical applications of functional nanomaterials.

Hongwei Duan is an associate professor in the School of Chemical and Biomedical Engineering at Nanyang Technological University (NTU). He received his B.S. in applied chemistry and M.S. in polymer chemistry & physics at Fudan University. After completing his Ph.D. with Prof. Helmuth Möhwald at the Max Planck Institute of Colloids and Interfaces, he had his postdoctoral training with Prof. Shuming Nie in the joint Department of Biomedical Engineering at Emory University and Georgia Institute of Technology. He joined NTU as a Nanyang Assistant Professor in 2009. His current research focuses on developing new chemistry towards nanostructures with structurally integrated inorganic nanocrystals and polymers and new approaches towards well-defined multifunctional assemblies of nanoscale building blocks and exploring the emerging optical, electronic, magnetic, catalytic, and structural properties of these materials for biomedical and environmental applications.

Xiaoyuan (Shawn) Chen earned his Ph.D. in chemistry from the University of Idaho in 1999. After two quick postdoctoral stays at Syracuse University and Washington University in St. Louis, he joined the University of Southern California as an Assistant Professor of Radiology. He then moved to Stanford University in 2004. He was promoted to Associate Professor in 2008, and in the summer of 2009, he joined the intramural research program of NIBIB/NIH, as a senior investigator and chief of the Laboratory of Molecular Imaging and Nanomedicine (LOMIN). Dr. Chen has published over 450 papers, 4 books, and numerous book chapters. He is the founding editor of the journal *Theranostics*.

DOI: 10.1021/acs.accounts.5b00059
Acc. Chem. Res. 2015, 48, 2506−2515

REFERENCES

(1) Hutter, E.; Fendler, J. H. Exploitation of Localized Surface Plasmon Resonance. *Adv. Mater.* **2004**, *16*, 1685−1706.
(2) Halas, N. J.; Lal, S.; Chang, W.-S.; Link, S.; Nordlander, P. Plasmons in Strongly Coupled Metallic Nanostructures. *Chem. Rev.* **2011**, *111*, 3913−3961.
(3) Morton, S. M.; Silverstein, D. W.; Jensen, L. Theoretical Studies of Plasmonics using Electronic Structure Methods. *Chem. Rev.* **2011**, *111*, 3962−3994.
(4) Saha, K.; Agasti, S. S.; Kim, C.; Li, X.; Rotello, V. M. Gold Nanoparticles in Chemical and Biological Sensing. *Chem. Rev.* **2012**, *112*, 2739−2779.
(5) Graham, D.; Thompson, D. G.; Smith, W. E.; Faulds, K. Control of enhanced Raman scattering using a DNA-based assembly process of dye-coded nanoparticles. *Nat. Nanotechnol.* **2008**, *3*, 548−551.
(6) Klinkova, A.; Choueiri, R. M.; Kumacheva, E. Self-assembled plasmonic nanostructures. *Chem. Soc. Rev.* **2014**, *43*, 3976−3991.
(7) Halas, N. J. Plasmonics: An Emerging Field Fostered by Nano Letters. *Nano Lett.* **2010**, *10*, 3816−3822.
(8) Odom, T. W.; Schatz, G. C. Introduction to Plasmonics. *Chem. Rev.* **2011**, *111*, 3667−3668.
(9) Tao, A. R.; Habas, S.; Yang, P. D. Shape control of colloidal metal nanocrystals. *Small* **2008**, *4*, 310−325.
(10) Cobley, C. M.; Chen, J. Y.; Cho, E. C.; Wang, L. V.; Xia, Y. N. Gold nanostructures: a class of multifunctional materials for biomedical applications. *Chem. Soc. Rev.* **2011**, *40*, 44−56.
(11) Giljohann, D. A.; Seferos, D. S.; Daniel, W. L.; Massich, M. D.; Patel, P. C.; Mirkin, C. A. Gold Nanoparticles for Biology and Medicine. *Angew. Chem., Int. Ed.* **2010**, *49*, 3280−3294.
(12) Jain, P. K.; Huang, X. H.; El-Sayed, I. H.; El-Sayed, M. A. Noble Metals on the Nanoscale: Optical and Photothermal Properties and Some Applications in Imaging, Sensing, Biology, and Medicine. *Acc. Chem. Res.* **2008**, *41*, 1578−1586.
(13) Huang, X. H.; Jain, P. K.; El-Sayed, I. H.; El-Sayed, M. A. Plasmonic photothermal therapy (PPTT) using gold nanoparticles. *Laser Med. Sci.* **2008**, *23*, 217−228.
(14) Nie, L.; Wang, S.; Wang, X.; Rong, P.; Ma, Y.; Liu, G.; Huang, P.; Lu, G.; Chen, X. In Vivo Volumetric Photoacoustic Molecular Angiography and Therapeutic Monitoring with Targeted Plasmonic Nanostars. *Small* **2014**, *10*, 1585−1593.
(15) Nie, L.; Chen, X. Structural and functional photoacoustic molecular tomography aided by emerging contrast agents. *Chem. Soc. Rev.* **2014**, *43*, 7132−7170.
(16) Huang, X. H.; El-Sayed, I. H.; Qian, W.; El-Sayed, M. A. Cancer cell imaging and photothermal therapy in the near-infrared region by using gold nanorods. *J. Am. Chem. Soc.* **2006**, *128*, 2115−2120.
(17) Jain, P. K.; El-Sayed, M. A. Universal scaling of plasmon coupling in metal nanostructures: Extension from particle pairs to nanoshells. *Nano Lett.* **2007**, *7*, 2854−2858.
(18) Hore, M. J. A.; Composto, R. J. Nanorod Self-Assembly for Tuning Optical Absorption. *ACS Nano* **2010**, *4*, 6941−6949.
(19) Choi, W. I.; Kim, J.-Y.; Kang, C.; Byeon, C. C.; Kim, Y. H.; Tae, G. Tumor Regression In Vivo by Photothermal Therapy Based on Gold-Nanorod-Loaded, Functional Nanocarriers. *ACS Nano* **2011**, *5*, 1995−2003.
(20) Huang, X. H.; Neretina, S.; El-Sayed, M. A. Gold Nanorods: From Synthesis and Properties to Biological and Biomedical Applications. *Adv. Mater.* **2009**, *21*, 4880−4910.
(21) Wang, X.; Qian, X. M.; Beitler, J. J.; Chen, Z. G.; Khuri, F. R.; Lewis, M. M.; Shin, H. J. C.; Nie, S. M.; Shin, D. M. Detection of Circulating Tumor Cells in Human Peripheral Blood Using Surface-Enhanced Raman Scattering Nanoparticles. *Cancer Res.* **2011**, *71*, 1526−1532.
(22) Kneipp, J.; Kneipp, H.; Kneipp, K. SERS-a single-molecule and nanoscale tool for bioanalytics. *Chem. Soc. Rev.* **2008**, *37*, 1052−1060.
(23) Yin, J.; Wu, T.; Song, J.; Zhang, Q.; Liu, S.; Xu, R.; Duan, H. SERS-Active Nanoparticles for Sensitive and Selective Detection of Cadmium Ion (Cd^{2+}). *Chem. Mater.* **2011**, *23*, 4756−4764.
(24) Song, J.; Duan, B.; Wang, C.; Zhou, J.; Pu, L.; Fang, Z.; Wang, P.; Lim, T. T.; Duan, H. SERS-Encoded Nanogapped Plasmonic Nanoparticles: Growth of Metallic Nanoshell by Templating Redox-Active Polymer Brushes. *J. Am. Chem. Soc.* **2014**, *136*, 6838−6841.
(25) Kim, N. H.; Lee, S. J.; Moskovits, M. Reversible Tuning of SERS Hot Spots with Aptamers. *Adv. Mater.* **2011**, *23*, 4152−4156.
(26) Qian, X.; Peng, X.-H.; Ansari, D. O.; Yin-Goen, Q.; Chen, G. Z.; Shin, D. M.; Yang, L.; Young, A. N.; Wang, M. D.; Nie, S. In vivo tumor targeting and spectroscopic detection with surface-enhanced Raman nanoparticle tags. *Nat. Biotechnol.* **2008**, *26*, 83−90.
(27) Lim, D.-K.; Jeon, K.-S.; Hwang, J.-H.; Kim, H.; Kwon, S.; Suh, Y. D.; Nam, J.-M. Highly uniform and reproducible surface-enhanced Raman scattering from DNA-tailorable nanoparticles with 1-nm interior gap. *Nat. Nanotechnol.* **2011**, *6*, 452−460.
(28) Reinhard, B. M.; Siu, M.; Agarwal, H.; Alivisatos, A. P.; Liphardt, J. Calibration of Dynamic Molecular Rulers Based on Plasmon Coupling between Gold Nanoparticles. *Nano Lett.* **2005**, *5*, 2246−2252.
(29) Mai, Y.; Eisenberg, A. Controlled Incorporation of Particles into the Central Portion of Vesicle Walls. *J. Am. Chem. Soc.* **2010**, *132*, 10078−10084.
(30) Murthy, V. S.; Cha, J. N.; Stucky, G. D.; Wong, M. S. Charge-Driven Flocculation of Poly(l-lysine)Gold Nanoparticle Assemblies Leading to Hollow Microspheres. *J. Am. Chem. Soc.* **2004**, *126*, 5292−5299.
(31) Pornpattananangkul, D.; Zhang, L.; Olson, S.; Aryal, S.; Obonyo, M.; Vecchio, K.; Huang, C.-M.; Zhang, L. Bacterial Toxin-Triggered Drug Release from Gold Nanoparticle-Stabilized Liposomes for the Treatment of Bacterial Infection. *J. Am. Chem. Soc.* **2011**, *133*, 4132−4139.
(32) Li, Y.; Smith, A. E.; Lokitz, B. S.; McCormick, C. L. In Situ Formation of Gold-"Decorated" Vesicles from a RAFT-Synthesized, Thermally Responsive Block Copolymer§. *Macromolecules* **2007**, *40*, 8524−8526.
(33) Rasch, M. R.; Rossinyol, E.; Hueso, J. L.; Goodfellow, B. W.; Arbiol, J.; Korgel, B. A. Hydrophobic Gold Nanoparticle Self-Assembly with Phosphatidylcholine Lipid: Membrane-Loaded and Janus Vesicles. *Nano Lett.* **2010**, *10*, 3733−3739.
(34) Song, J.; Pu, L.; Zhou, J.; Duan, B.; Duan, H. Biodegradable Theranostic Plasmonic Vesicles of Amphiphilic Gold Nanorods. *ACS Nano* **2013**, *7*, 9947−9960.
(35) Song, J.; Cheng, L.; Liu, A.; Yin, J.; Kuang, M.; Duan, H. Plasmonic Vesicles of Amphiphilic Gold Nanocrystals: Self-Assembly and External-Stimuli-Triggered Destruction. *J. Am. Chem. Soc.* **2011**, *133*, 10760−10763.
(36) Song, J.; Zhou, J.; Duan, H. Self-Assembled Plasmonic Vesicles of SERS-Encoded Amphiphilic Gold Nanoparticles for Cancer Cell Targeting and Traceable Intracellular Drug Delivery. *J. Am. Chem. Soc.* **2012**, *134*, 13458−13469.
(37) Song, J.; Fang, Z.; Wang, C.; Zhou, J.; Duan, B.; Pu, L.; Duan, H. Photolabile Plasmonic Vesicles Assembled from Amphiphilic Gold Nanoparticles for Remote-Controlled Traceable Drug Delivery. *Nanoscale* **2013**, *5*, 5816−5824.
(38) Lin, J.; Wang, S.; Huang, P.; Wang, Z.; Chen, S.; Niu, G.; Li, W.; He, J.; Cui, D.; Lu, G.; Chen, X.; Nie, Z. Photosensitizer-Loaded Gold Vesicles with Strong Plasmonic Coupling Effect for Imaging-Guided Photothermal/Photodynamic Therapy. *ACS Nano* **2013**, *7*, 5320−5329.
(39) Huang, P.; Lin, J.; Li, W.; Rong, P.; Wang, Z.; Wang, S.; Wang, X.; Sun, X.; Aronova, M.; Niu, G.; Leapman, R. D.; Nie, Z.; Chen, X. Biodegradable Gold Nanovesicles with an Ultrastrong Plasmonic Coupling Effect for Photoacoustic Imaging and Photothermal Therapy. *Angew. Chem., Int. Ed.* **2013**, *52*, 13958−13964.
(40) He, J.; Huang, X.; Li, Y.-C.; Liu, Y.; Babu, T.; Aronova, M. A.; Wang, S.; Lu, Z.; Chen, X.; Nie, Z. Self-Assembly of Amphiphilic Plasmonic Micelle-Like Nanoparticles in Selective Solvents. *J. Am. Chem. Soc.* **2013**, *135*, 7974−7984.

DOI: 10.1021/acs.accounts.5b00059
Acc. Chem. Res. 2015, 48, 2506−2515

(41) He, J.; Liu, Y.; Babu, T.; Wei, Z.; Nie, Z. Self-Assembly of Inorganic Nanoparticle Vesicles and Tubules Driven by Tethered Linear Block Copolymers. *J. Am. Chem. Soc.* **2012**, *134*, 11342−11345.
(42) Cheng, L.; Song, J.; Yin, J.; Duan, H. Self-Assembled Plasmonic Dimers of Amphiphilic Gold Nanocrystals. *J. Phys. Chem. Lett.* **2011**, *2*, 2258−2262.
(43) Cheng, L.; Liu, A. P.; Peng, S.; Duan, H. W. Responsive Plasmonic Assemblies of Amphiphilic Nanocrystals at Oil-Water Interfaces. *ACS Nano* **2010**, *4*, 6098−6104.
(44) Zubarev, E. R.; Xu, J.; Sayyad, A.; Gibson, J. D. Amphiphilic Gold Nanoparticles with V-Shaped Arms. *J. Am. Chem. Soc.* **2006**, *128*, 4958−4959.
(45) Kim, J.-B.; Bruening, M. L.; Baker, G. L. Surface-Initiated Atom Transfer Radical Polymerization on Gold at Ambient Temperature. *J. Am. Chem. Soc.* **2000**, *122*, 7616−7617.
(46) Theato, P. Synthesis of well-defined polymeric activated esters. *J. Polym. Sci., Part A: Polym. Chem.* **2008**, *46*, 6677−6687.
(47) He, J.; Zhang, P.; Babu, T.; Liu, Y.; Gong, J.; Nie, Z. Near-infrared light-responsive vesicles of Au nanoflowers. *Chem. Commun.* **2013**, *49*, 576−578.
(48) Discher, D. E.; Eisenberg, A. Polymer vesicles. *Science* **2002**, *297*, 967−973.
(49) Al-Jamal, W. T.; Kostarelos, K. Liposomes: From a Clinically Established Drug Delivery System to a Nanoparticle Platform for Theranostic Nanomedicine. *Acc. Chem. Res.* **2011**, *44*, 1094−1104.
(50) Alvarez-Puebla, R. A.; Liz-Marzán, L. M. SERS-Based Diagnosis and Biodetection. *Small* **2010**, *6*, 604−610.
(51) Qian, X.; Li, J.; Nie, S. Stimuli-Responsive SERS Nanoparticles: Conformational Control of Plasmonic Coupling and Surface Raman Enhancement. *J. Am. Chem. Soc.* **2009**, *131*, 7540−7541.
(52) Abramczyk, H.; Brozek-Pluska, B.; Surmacki, J.; Jablonska-Gajewicz, J.; Kordek, R. Raman 'optical biopsy' of human breast cancer. *Prog. Biophys. Mol. Biol.* **2012**, *108*, 74−81.
(53) Abramczyk, H.; Brozek-Pluska, B.; Surmacki, J.; Jablonska, J.; Kordek, R. The Label-Free Raman Imaging of Human Breast Cancer. *J. Mol. Liq.* **2011**, *164*, 123−131.

DOI: 10.1021/acs.accounts.5b00059
Acc. Chem. Res. 2015, 48, 2506−2515